

# Topologically protected negative entanglement

Wen-Tan Xue<sup>1</sup> and Ching Hua Lee<sup>1</sup>

<sup>1</sup>Department of Physics, National University of Singapore, Singapore 117542

The entanglement entropy encodes fundamental characteristics of quantum many-body systems, and is particularly subtle in non-Hermitian settings where eigenstates generically become non-orthogonal. In this work, we find that negative biorthogonal entanglement generically arises from topologically-protected non-orthogonal edge states in free fermion systems, especially within topological flat bands. Departing from previous literature which associated negative entanglement with exceptional gapless points, we show that robustly negative entanglement can still occur in gapped systems. Gapless 2D topological flat bands, however, exhibits novel  $S \sim -L_z^2 \log L$  entanglement behavior which scales quadratically with the transverse dimension  $L_z$ . Our discovery sheds light on a new interplay between topology and entanglement unrelated to traditional concepts of topological entanglement entropy.

**Introduction.**— The entanglement entropy plays a crucial role in unveiling fundamental insights into the locality of quantum information. For instance, by scaling either according to the volume or area [1, 2], the entanglement entropy reveals whether quantum correlations pervade the entire system or remain localized. Intriguingly, numerous studies [3–5] have suggested that the presence of topological order can also be encoded in the entanglement entropy, as revealed by the presence of an additional constant term [6] or discontinuities [7] in the scaling relation.

In this work, extending into the non-Hermitian realm[8–16], we uncover a new manner in which topology can substantially influence entanglement entropy behavior. Specifically, we show that certain topological boundary states can exert a strongly non-local influence on the dominant entanglement behavior of the *entire* system, such that the entanglement entropy of free fermions scales negatively with the system size. A key consequence of non-Hermiticity is that the eigenstates of the Hamiltonian  $H$  are generically no longer orthogonal, such that a biorthogonal basis with left and right eigenstates i.e.  $H = \sum E_n |\psi_n^R\rangle \langle \psi_n^L|$  with  $\langle \psi_m^L | \psi_n^R \rangle = \delta_{mn}$  is needed to maintain orthogonality and retain the probabilistic interpretation of quantum mechanics[17, 18]. Within this biorthogonal framework, recent studies have revealed that both bipartite entanglement entropy and Rényi entropy can manifest unexpected negative values [19–22]. These studies attribute the negativity to the presence of geometric defectiveness at exceptional points (EPs) [19, 21].

A key discovery in this work is that the presence of an EP is strictly not a prerequisite for observing negative entanglement entropy values – instead, substantial non-orthogonality among the right eigenstates suffices, and spectacularly so when the non-orthogonality is enforced by a topological flatband. We explore two two-dimensional (2D) topological non-Hermitian models and unveil a remarkable phenomenon: the topological edge (right) states in these models demonstrate a significant overlap, approaching 1, while the overlap among bulk states remains minimal. Consequently, the topological characteristics can be strategically employed to switch the negative entanglement entropy on or off. Most notably, for the second model, when  $b_0 = 1$ , the system’s non-trivial topology leads to a pronounced negative scaling of the entanglement

entropy with system size, following a novel quadratic relation  $S \propto -L_z^2 \log L$ . These two models elucidate how topological protection mechanisms underpin the observed negative entanglement entropy, offering profound insights into the interplay between quantum entanglement and topological phases.

**Negative entanglement from eigenstate non-orthogonality.**— In the non-Hermitian context, the density operator that preserves its role as a probabilistic weight is the biorthogonal density matrix  $\rho = |\Psi^R\rangle \langle \Psi^L|$ , where

$$|\Psi^R\rangle = \prod_{n \in occ} \psi_{Rn}^\dagger |0\rangle, \quad |\Psi^L\rangle = \prod_{n \in occ} \psi_{Ln}^\dagger |0\rangle \quad (1)$$

are the right and left many-body ground states created by bifermionic creation operators  $\psi_{Rn}^\dagger, \psi_{Ln}^\dagger$  satisfying  $\{\psi_{Lm}, \psi_{Rn}^\dagger\} = \delta_{mn}$ , such that  $\langle \Psi^L | \Psi^R \rangle = 1, \langle \Psi^R | \Psi^R \rangle \neq 1, \langle \Psi^L | \Psi^L \rangle \neq 1$ . We specialize to free boson and fermion systems, where the ground state and thermal states are Gaussian states. As such, all correlation functions adhere to Wick’s theorem, and the reduced density matrix  $\rho_A$  corresponding to an entanglement subregion  $A$  is completely expressible [23] in terms of the two-point function  $\langle c_{x_1}^\dagger c_{x_2} \rangle = \langle x_1 | P | x_2 \rangle = L^{-1} \sum_k e^{ik(x_1 - x_2)} P(k)$ , where [21]  $P(k) = \sum_{n \in occ} |\psi_n^R(k)\rangle \langle \psi_n^L(k)|$  projects to the occupied bands  $n$ , with  $k$  the momentum index. To enforce the entanglement cut, we also introduce  $\Gamma_A$  to be the real-space projector onto subregion  $A$ , such that the  $A$ -truncated band projector takes the form

$$\bar{P} = \Gamma_A P \Gamma_A = \sum_{n \in occ} \Gamma_A |\psi_n^R\rangle \langle \psi_n^L| \Gamma_A = \sum_{n \in occ} |\psi_{nA}^R\rangle \langle \psi_{nA}^L|. \quad (2)$$

Crucially, this  $\bar{P}$  operator crucially contain complete information of the  $n$ th-order Rényi entropy for free fermions [24]

$$\begin{aligned} S_A^{(n)} &= \frac{\log \text{Tr}(\rho_A^n)}{1-n} = \frac{1}{1-n} \text{Tr} \left[ \log (\bar{P}^n + (I - \bar{P})^n) \right] \\ &= \frac{1}{1-n} \sum_i \log(p_i^n + (1-p_i)^n), \end{aligned} \quad (3)$$

which, in the limit of  $n \rightarrow 1$ , yields the von Neumann entropy

$$\begin{aligned} S_A &= -\text{Tr} \rho_A \log \rho_A = -\text{Tr} [\bar{P} \log \bar{P} + (I - \bar{P}) \log (I - \bar{P})] \\ &= \sum_{p_i} -p_i \log(p_i) - (1-p_i) \log(1-p_i), \end{aligned} \quad (4)$$

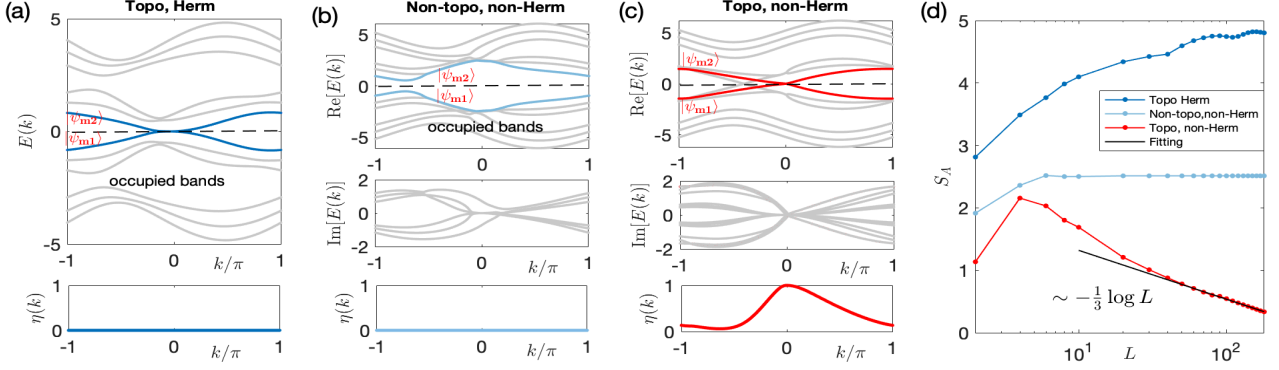


FIG. 1. Negative entanglement in the 4-band exceptional topological crossing model (Eq. (7)) under z-OBCs with  $L_z = 3$ . (a) In the topologically non-trivial but Hermitian case ( $\alpha = 0, M = 1.2, \delta = 0$ ), the squared overlap  $\eta(k)$  [Eq. (5)] of the topological eigenstates (blue) vanishes rigorously. (b) In the topologically trivial (gapped), non-Hermitian case ( $\alpha = 0.5\pi, M = 3, \delta = 2$ ),  $\eta(k)$  of the closest bulk states (light blue) still vanishes essentially. (c) For the non-trivial Chern case ( $\alpha = 0, M = 3, \delta = 2$ ), perfect overlap i.e.  $\eta(k) = 1$  is reached where topological edge modes (red) cross. (d) The free fermion entanglement entropy  $S_A$  for cases (a,b) respectively increases and saturates with system circumference  $L$  as expected, but that from the topological exceptional crossing (c) exhibits a new  $-\frac{1}{3} \log L$  scaling. The entanglement subregion is taken to be the width- $L/2$  half-cylinder.

where  $I$  is the identity matrix and  $p_i$  are the eigenvalues of  $\bar{P}$ . Physically,  $p_i$  represents occupation probabilities subject to the restriction to subregion  $A$ , and are indeed real and within  $[0, 1]$  for Hermitian  $H$ . But in non-Hermitian settings, due to gain/loss either onsite or across the subregion boundary, we can potentially have  $p_i \gg 1$ , as we shall show shortly. Importantly,  $p_i > 1$  contributes negatively to both  $S_A^{(n>1)}$  and  $S_A = \lim_{n \rightarrow 1} S_A^{(n)}$  entropies, as elaborated in the Supplement[25].

Below, we show that having strong eigenstate overlap gives rise to large  $p_i$  that in turn results in negative Rényi and entanglement entropy. For any pair of non-orthogonal right eigenstates  $|\psi_m^R\rangle$  and  $|\psi_n^R\rangle$ , their normalized squared overlap [26]

$$\eta = \frac{|\langle \psi_m^R | \psi_n^R \rangle|^2}{\langle \psi_m^R | \psi_m^R \rangle \langle \psi_n^R | \psi_n^R \rangle} = \frac{(U^\dagger U)_{mn}^2}{(U^\dagger U)_{mm} (U^\dagger U)_{nn}} \neq 0 \quad (5)$$

does not vanish. Here we have introduced the matrix  $U$  whose elements are the real space components of the right eigenstates i.e.  $|\psi_n^R\rangle = \sum_i U_{in} |i\rangle$ , such that the corresponding matrix for the left eigenstates is  $U^{-1}$  i.e.  $\langle \psi_m^L | = \sum_i (U^{-1})_{mi} \langle i |$ . In the extreme limit where the two eigenstates become parallel,  $\eta \rightarrow 1$  and the rank of  $U^\dagger U$  becomes lower than the dimension of the space of occupied states. This leads to the vanishing of  $\text{Det}(U)$  and crucially forces  $U^{-1}$  to acquire very large matrix elements. From

$$\begin{aligned} \sum_i p_i^2 &= \text{Tr}(\bar{P}^2) = \sum_{m,n \in \text{occ}} \langle \psi_m^L | \Gamma_A | \psi_n^R \rangle \langle \psi_n^L | \Gamma_A | \psi_m^R \rangle \\ &= \sum_{m,n \in \text{occ}} (U^{-1} \Gamma_A U)_{mn} (U^{-1} \Gamma_A U)_{nm} \end{aligned} \quad (6)$$

where we have used  $\Gamma_A^2 = \Gamma_A$ , we deduce that at least one of the  $p_i$  must also have become very large, since the divergent elements in  $U^{-1}$  do not in general cancel off with the small elements in  $\Gamma_A U^{-1}$  except in the case of vanishing entanglement cut  $\Gamma_A = I$ . However, we stress that even when  $U^\dagger U$  is

still full-rank with non-defective eigenspace,  $\eta$  can already be extremely close to unity and contribute to negative entanglement.

*Exceptional topological crossing.*— In this section and the next, we showcase two illustrative 2D systems where topologically protected edge states with  $\eta \approx 1$  contribute negative entanglement to different degrees of success. We consider a cylindrical geometry such that the  $z$  direction contains  $L_z$  unit cells, and is bounded so as to host topological edge states. The other translation-invariant (circumferential) direction contains  $L$  unit cells, and we shall assign half i.e.  $L/2$  of it to be the entanglement subregion  $A$ .  $P(k)$  projects onto the occupied lower half bands with  $\text{Re}[E(k)] < E_F = 0$  unless otherwise stated.

First, we showcase a model with topological edge modes that intersect at an exceptional crossing. Unlike typical topological band crossings where the topological modes just have to be energetically degenerate, here we require them to also coalesce i.e. become parallel. This requires at least four topological edge modes, since there has to be at least two completely overlapping topological modes at each of the two edges. A candidate model is given by the following 4-band Hamiltonian

$$\begin{aligned} \mathcal{H}(k, k_z) &= (\cos k_z - \sin k - M) \tau_x \sigma_0 \\ &+ \tau_y (\cos k \sigma_x - \sigma_y + \sin k_z \sigma_z) \\ &+ (\sin \alpha \tau_0 + \cos \alpha \tau_x) \sum_{\mu=x,y,z} \sigma_\mu + i \delta \tau_y \sigma_0. \end{aligned} \quad (7)$$

where the  $\sigma_\mu$  and  $\tau_\mu$  Pauli matrices act in spin and sublattice space respectively. The first term controls the band inversion through  $M$ , the second term represents the spin-orbit coupling which break time-reversal, and the third term introduces a Zeeman field that can also involve sublattice hoppings. The final term,  $i \delta \tau_y \sigma_0$ , introduces non-Hermiticity through sublattice hopping asymmetry.

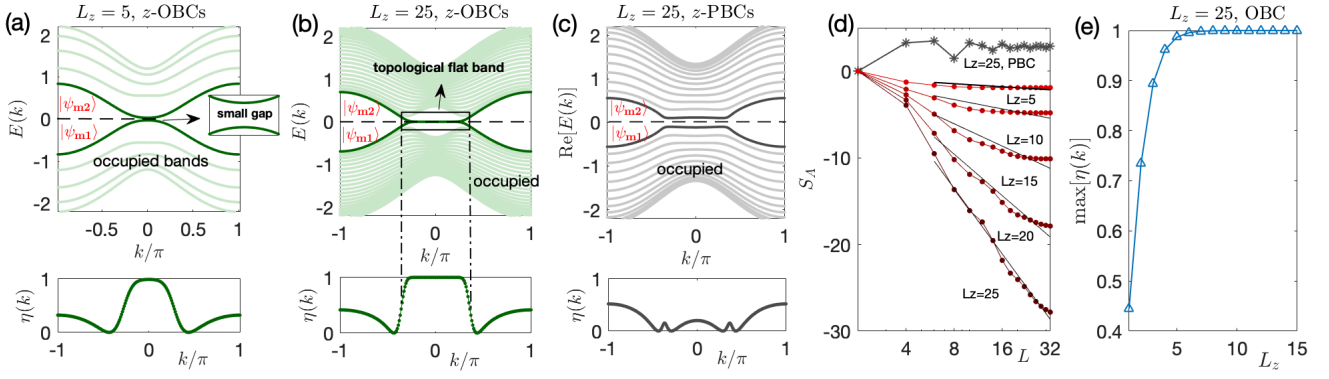


FIG. 2. Analysis for the 2-band Hamiltonian (Eq. (9)) with parameters:  $b_0 = 1.2 \neq 1, B = 1, t = 0.8, a_0 = 1$ . (a) Energy spectrum  $E(k)$  and the overlap factor  $\eta(k)$  for small  $L_z = 5$ , under OBC in  $z$  direction. (b) Upon increasing the system size to  $L_z = 25$ , the emergence of a topological flat band is observed within the non-trivial regime prescribed by Eq. (10), with  $\eta(k) \approx 1$  characterizing this regime. (c) With  $z$ -direction PBCs, the topological flatband disappears and so does  $\eta = 1$ , even though the gap is still small. (d) The scaling behavior of  $S_A$  for system lengths  $L \in [2, 32]$ . Notably, as  $L_z$  increases,  $S_A$  exhibits a more pronounced decrease. (e) The maximum value of  $\eta(k)$  with  $L_z$ , which is almost nearly unity for  $L_z \geq 10$ .

In Fig. 1, we present three distinct scenarios corresponding to different parameter combinations, focusing particularly on the overlap  $\eta(k)$  between the middle two eigenstates which straddle the Fermi energy  $E_F = 0$  (dashed line). Open boundary conditions (OBCs) are taken only along the  $z$  direction, such that  $k$  remains a good quantum number. In Fig. 1(a) with intersecting Hermitian topological modes (blue),  $\eta(k) = 0$  due to the exact orthonormality of Hermitian eigenstates. In Fig. 1(b) which is non-Hermitian ( $\delta \neq 0$ ),  $\eta(k)$  remains essentially zero due to the substantial bulk gap. However, in the non-Hermitian case with topological modes [Fig. 1(c)], the topological edge modes (red) cross and coalesce, forming an exceptional point, as reflected by the saturated squared overlap of  $\eta(0) = 1$ . Only for this exceptional topological case do we see negatively entanglement entropy  $S_A$  [Fig. 1(d)]; for the previous two gapless and gapped cases of Figs. 1(a/b),  $S_A$  respectively grows/saturates with  $L$  as expected from usual conformal field theory [27–31].

Empirically, the

$$\text{Re}S_A \sim -0.3399 \log L \approx \left(\frac{1}{3} - \frac{2}{3}\right) \log L, \quad (8)$$

scaling in the exceptional topological case differs from the previously reported  $S_A \sim -\frac{2}{3} \log L$  scaling for a linearly dispersive exceptional point [19, 21, 22]. This discrepancy is attributed to gapless non-exceptional gapless crossing [Gray in Figs. 1(c)], which contribute the usual  $\frac{1}{3} \log L$  entanglement. As such, the negative entanglement from exceptional topological crossings can be easily overshadowed by other non-exceptional topological crossings, and is in this sense not necessarily robust [32].

*Enhanced negative entanglement from topological flat bands.*— We next depart from the exceptional topological crossing paradigm and demonstrate how topological flat bands can give rise to much stronger negative entanglement, even if the bands are not strictly gapless or defective. To realize pro-

tected flat band across an extended range of  $k$ , we consider the Hamiltonian

$$H(k, k_z) = \begin{pmatrix} 0 & te^{-ik_z} + a_0 \\ te^{ik_z} + (b_0 - \cos k)^B & 0 \end{pmatrix}, \quad (9)$$

with  $k$ -dependent asymmetric off-diagonal hoppings, where  $a_0, b_0, B > 0$  are all real. Under  $z$ -direction OBCs, the non-Hermitian effect enhances the edge localization with a skin depth of  $-2/\log[(b_0 - \cos k)^B/a_0]$  and dynamically induces a real energy spectrum from non-Bloch PT-symmetry [33–41]. Almost-flat topological bands exist whenever

$$|a_0(b_0 - \cos k)^B| \leq t^2, \quad (10)$$

although they are *not necessarily* gapless for any  $L_z$ : Employing Schur’s determinant identity on the real-space Hamiltonian  $[H_{1D}(k)]_{ij} = (2\pi)^{-1} \int e^{ik_z(z_1 - z_2)} H(k, k_z) dk_z$ , as elaborated in the Supplement [25], we have

$$\det[H_{1D}(k)] = [a_0(b_0 - \cos k)^B]^{L_z}, \quad (11)$$

implying that for  $0 < |a_0(b_0 - \cos k)^B| < 1$ , the topological gap approaches zero as  $L_z \rightarrow \infty$ , but never exactly closes. Perfect gap closure is only possible for  $b_0 \leq 1$ , and below we investigate these two cases separately.

*1. Gapped flat bands ( $b_0 > 1$ )*— An intriguing observation, as depicted in Fig. 2(b), is that with an increase in  $L_z$ , the energy gap narrows, leading to the emergence of a topological flat band within the non-trivial regime defined by Eq. (10). This regime is characterized by an overlap factor  $\eta(k) \approx 1$  across the entire flat band, suggesting that states within an extensive continuum of  $k$  closely approximate EPs, even if they are not technically EP crossings. This finding is particularly unexpected since the Hamiltonian  $H(k, k_z)$  in Eq. (9) does not inherently feature EPs. Instead, these quasi-EPs arise solely due to the presence of topological edge states. As a comparison, for periodic boundary conditions (PBCs) in the  $z$  direction

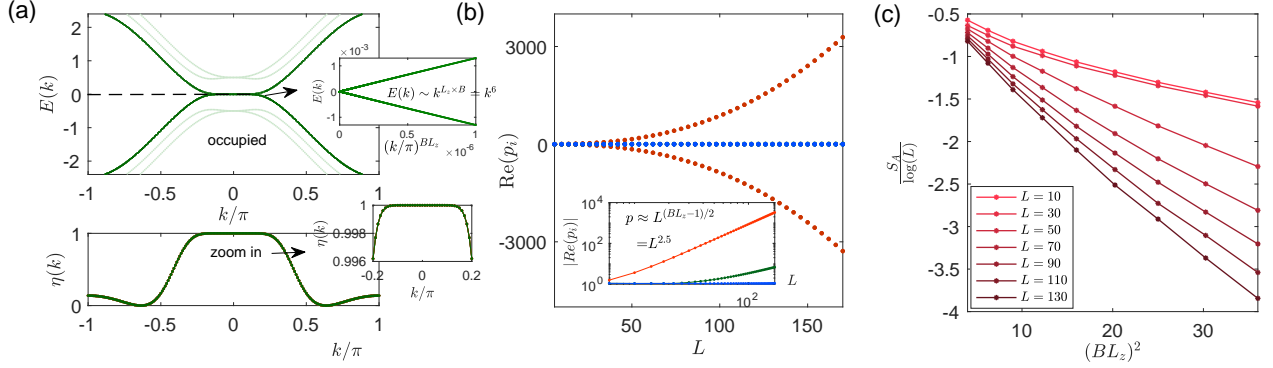


FIG. 3. Analysis for the 2-band Hamiltonian (Eq. (9)) with parameters:  $b_0 = 1, B = 2, t = 0.5, a_0 = 2$ . (a) Energy spectrum under OBC with  $L_z = 3$ , with dispersion  $E(k) \sim k^{BL_z}$  around  $k = 0$  ( $k \in [0, 0.1\pi]$ ). (b) The power law scaling of the eigenvalues of  $\bar{P}$  with  $L$ . We observe the emergence of the first-order, second and higher-order states, as  $L$  increases. (c) The scaling behavior of  $S_A$ . Notably, for a large  $L$ ,  $S_A$  is linearly proportional to  $(BL_z)^2$ , aligning with the theoretical prediction in Eq. (13).

[Fig. 2(c)], the topological flat band is absent, and the overlap  $\eta$  does not approach one even as  $L_z$  increased to 25, such that the (bulk) band gap becomes quite narrow.

The bipartite entanglement entropy,  $S_A$ , as shown in Fig. 2(d), exhibits an increasingly steep decay with  $L$  as  $L_z$  increased. For a small  $L_z=5$ , a closer inspection reveals an initial decay in  $\text{Re}[S(L, L/2)]$  with  $L$ , which then stabilizes as a constant negative value. This is attributed to the finite energy gap at  $k = 0$ , wherein the overlap at  $k_0 = \pi/L$  (nearest point to  $k = 0$ ) does not infinitely approach 1 with increasing  $L$ . Additionally, the grey star line in Fig. 2(d) indicates that  $S_A$  remains constant under PBC case, consistent with the gapped spectrum observed.

**2. Gapless flat bands ( $b_0 = 1$ )** – In this subsection, we focus on the case of  $b_0 = 1$ , which is the simplest case for which the flat band is gapless. According to Eq.(11), this leads to  $\det[H_{1D}(k)] = 0$  at  $k = 0$ , implying that  $k = 0$  is a strict EP. Fascinatingly, as illustrated in Fig. 3(a) and proven in the Supplement[25], the edge bands around the EP demonstrate a very high-order dispersion, described by  $E_s(k) \sim k^{B \times L_z}$  where  $L_z$  denotes the system length in the  $z$ -direction, and  $B$  is the power in  $H(k, k_z)$ . As shown in Fig. 3(b), this higher-power dispersion results in the eigenvalues  $p_i$  of  $\bar{P}$  significantly exceed  $[0, 1]$  interval (red dots). Specifically, as shown in the inset of Fig. 3(b)) corresponding to different powers. These branches represent the first, second, and higher-order eigenstates of  $\bar{P}$ . As derived in the Supplement[25], by expanding  $(b_0 - \cos k)^B$  in various orders of  $k$ , we arrive at a whole hierarchy of large  $p_i$  eigenvalues: the eigenvalue for the first order state satisfies  $p_i \sim L^{(BL_z-1)/2}$ , while the second order follows  $p_i \sim L^{(BL_z-1)/2-1}$ , with subsequent higher orders diminishing until the exponent becomes negative.

As derived in the Supplemental, for the eigenvalues  $p_i \sim L^\alpha$ , the real part of the entanglement entropy scales as  $S_A \sim$

$-\alpha \log(L)$ . Therefore, the first-order states contribute as

$$S_A^{\text{1st-order}} \sim -\frac{BL_z - 1}{2} \log L. \quad (12)$$

As seen in the inset of Fig. 3(b), for smaller  $L$ , the entanglement entropy primarily arises from the first-order states, indicating a linear proportionality to  $L_z$  and  $\log(L)$ . However, as  $L$  increases, contributions from second and higher-order states become unignorable, leading to an entanglement entropy of

$$\begin{aligned} S_A &\sim -\left(\frac{BL_z - 1}{2} + \frac{BL_z - 1}{2} - 1\right) \log L - \dots \\ &\sim -\frac{1}{2}(BL_z)^2 \log L, \end{aligned} \quad (13)$$

showcasing a quadratic relationship with  $L_z$ . Fig. 3(c) visually captures this transition from linear to quadratic scaling with  $L_z$  as  $L$  grows.

In all, the above results reveal that: 1) Non-trivial topology and the non-Hermitian skin effect induces an overlap of  $\eta(k) \rightarrow 1$  in the edge bands (quasi-EPs), forming a highly degenerate topological flat band. 2) The significant topologically-protected state overlap leads to negative entanglement entropy, even in the presence of a small gap.

- 
- [1] M. Srednicki, Entropy and area, *Phys. Rev. Lett.* **71**, 666 (1993).
  - [2] J. Eisert, M. Cramer, and M. B. Plenio, Colloquium: Area laws for the entanglement entropy, *Rev. Mod. Phys.* **82**, 277 (2010).
  - [3] A. Kitaev and J. Preskill, Topological entanglement entropy, *Phys. Rev. Lett.* **96**, 110404 (2006).
  - [4] H. Li and F. D. M. Haldane, Entanglement spectrum as a generalization of entanglement entropy: Identification of topological order in non-abelian fractional quantum hall effect states, *Phys. Rev. Lett.* **101**, 010504 (2008).
  - [5] M. Levin and X.-G. Wen, Detecting topological order in a ground state wave function, *Phys. Rev. Lett.* **96**, 110405 (2006).
  - [6] G. Vidal, J. I. Latorre, E. Rico, and A. Kitaev, Entanglement in quantum critical phenomena, *Phys. Rev. Lett.* **90**, 227902 (2003).



- [7] J. Cho and K. W. Kim, Quantum phase transition and entanglement in topological quantum wires, *Scientific Reports* **7**, 2745 (2017).
- [8] C. H. Lee and R. Thomale, Anatomy of skin modes and topology in non-hermitian systems, *Phys. Rev. B* **99**, 201103 (2019).
- [9] F. Song, S. Yao, and Z. Wang, Non-hermitian topological invariants in real space, *Phys. Rev. Lett.* **123**, 246801 (2019).
- [10] F. Song, S. Yao, and Z. Wang, Non-hermitian skin effect and chiral damping in open quantum systems, *Phys. Rev. Lett.* **123**, 170401 (2019).
- [11] S. Longhi, Probing non-hermitian skin effect and non-bloch phase transitions, *Phys. Rev. Res.* **1**, 023013 (2019).
- [12] K. Zhang, Z. Yang, and C. Fang, Correspondence between winding numbers and skin modes in non-hermitian systems, *Phys. Rev. Lett.* **125**, 126402 (2020).
- [13] K. Yokomizo and S. Murakami, Non-bloch band theory of non-hermitian systems, *Phys. Rev. Lett.* **123**, 066404 (2019).
- [14] Z. Yang, K. Zhang, C. Fang, and J. Hu, Non-hermitian bulk-boundary correspondence and auxiliary generalized brillouin zone theory, *Phys. Rev. Lett.* **125**, 226402 (2020).
- [15] F. Qin, Y. Ma, R. Shen, and C. H. Lee, Universal competitive spectral scaling from the critical non-hermitian skin effect, *Phys. Rev. B* **107**, 155430 (2023).
- [16] L. Li, S. Mu, C. H. Lee, and J. Gong, Quantized classical response from spectral winding topology, *Nature Communications* **12**, 5294 (2021).
- [17] D. C. Brody, Biorthogonal quantum mechanics, *Journal of Physics A: Mathematical and Theoretical* **47**, 035305 (2013).
- [18] S. Weigert, Completeness and orthonormality in PT-symmetric quantum systems, *Phys. Rev. A* **68**, 062111 (2003).
- [19] C. H. Lee, Exceptional bound states and negative entanglement entropy, *Phys. Rev. Lett.* **128**, 010402 (2022).
- [20] D. Zou, T. Chen, H. Meng, Y. S. Ang, X. Zhang, and C. H. Lee, Experimental observation of exceptional bound states in a classical circuit network (2023), [arXiv:2308.01970 \[quant-ph\]](https://arxiv.org/abs/2308.01970).
- [21] P.-Y. Chang, J.-S. You, X. Wen, and S. Ryu, Entanglement spectrum and entropy in topological non-hermitian systems and nonunitary conformal field theory, *Phys. Rev. Res.* **2**, 033069 (2020).
- [22] Y.-T. Tu, Y.-C. Tzeng, and P.-Y. Chang, Rényi entropies and negative central charges in non-Hermitian quantum systems, *SciPost Phys.* **12**, 194 (2022).
- [23] I. Peschel, Calculation of reduced density matrices from correlation functions, *Journal of Physics A: Mathematical and General* **36**, L205 (2003).
- [24] An analogous expression also holds for free bosons:  $S_{A,boson}^{(n)} = \frac{1}{n-1} \text{Tr} \left[ \log \left( \bar{P}^n - (\bar{P} - I)^n \right) \right]$ .
- [25] Supplemental material for "topologically protected negative entanglement".
- [26]  $\eta$  can be viewed as a variant of the Petermann factor [42–45].
- [27] C. Callan and F. Wilczek, On geometric entropy, *Physics Letters B* **333**, 55 (1994).
- [28] T. M. Fiola, J. Preskill, A. Strominger, and S. P. Trivedi, Black hole thermodynamics and information loss in two dimensions, *Phys. Rev. D* **50**, 3987 (1994).
- [29] C. Holzhey, F. Larsen, and F. Wilczek, Geometric and renormalized entropy in conformal field theory, *Nuclear Physics B* **424**, 443 (1994).
- [30] S. Hawking, J. Maldacena, and A. Strominger, Desitter entropy, quantum entanglement and ads/cft, *Journal of High Energy Physics* **2001**, 001 (2001).
- [31] P. Calabrese and J. Cardy, Entanglement entropy and quantum field theory, *Journal of Statistical Mechanics: Theory and Experiment* **2004**, P06002 (2004).
- [32] This is particularly so if the exceptional dispersion is square-root, as for some generalizations of our model[25].
- [33] C. M. Bender, M. V. Berry, and A. Mandilara, Generalized pt symmetry and real spectra, *Journal of Physics A: Mathematical and General* **35**, L467 (2002).
- [34] C. M. Bender, Making sense of non-hermitian hamiltonians, *Reports on Progress in Physics* **70**, 947 (2007).
- [35] H. Hodaie, M. A. Miri, A. U. Hassan, W. E. Hayenga, M. Heinrich, D. N. Christodoulides, and M. Khajavikhan, Parity-time-symmetric coupled microring lasers operating around an exceptional point, *Opt. Lett.* **40**, 4955 (2015).
- [36] L. Feng, Z. J. Wong, R.-M. Ma, Y. Wang, and X. Zhang, Single-mode laser by parity-time symmetry breaking, *Science* **346**, 972 (2014), <https://www.science.org/doi/pdf/10.1126/science.1258479>.
- [37] S. Yao and Z. Wang, Edge states and topological invariants of non-hermitian systems, *Phys. Rev. Lett.* **121**, 086803 (2018).
- [38] Z. Lei, C. H. Lee, and L. Li,  $\mathcal{PT}$ -activated non-hermitian skin modes (2023), [arXiv:2304.13955 \[cond-mat.mes-hall\]](https://arxiv.org/abs/2304.13955).
- [39] R. El-Ganainy, K. G. Makris, M. Khajavikhan, Z. H. Muslimani, S. Rotter, and D. N. Christodoulides, Non-hermitian physics and pt symmetry, *Nature Physics* **14**, 11 (2018).
- [40] Ş. K. Özdemir, S. Rotter, F. Nori, and L. Yang, Parity–time symmetry and exceptional points in photonics, *Nature Materials* **18**, 783 (2019).
- [41] C. E. Rüter, K. G. Makris, R. El-Ganainy, D. N. Christodoulides, M. Segev, and D. Kip, Observation of parity–time symmetry in optics, *Nature Physics* **6**, 192 (2010).
- [42] K. Petermann, Calculated spontaneous emission factor for double-heterostructure injection lasers with gain-induced waveguiding, *IEEE Journal of Quantum Electronics* **15**, 566 (1979).
- [43] Z. G. Yuto Ashida and M. Ueda, Non-hermitian physics, *Advances in Physics* **69**, 249 (2020), <https://doi.org/10.1080/00018732.2021.1876991>.
- [44] H. Wang, Y.-H. Lai, Z. Yuan, M.-G. Suh, and K. Vahala, Petermann-factor sensitivity limit near an exceptional point in a brillouin ring laser gyroscope, *Nature Communications* **11**, 1610 (2020).
- [45] Y.-Y. Zou, Y. Zhou, L.-M. Chen, and P. Ye, Detecting bulk and edge exceptional points in non-hermitian systems through generalized petermann factors, *Frontiers of Physics* **19**, 23201 (2023).